CDDpress

www.nature.com/cdd

ARTICLE OPEN

Spatial and functional characterization of ER stress proteins links fibroblast plasticity and proliferative processes in human osteoarthritic synovitis

Zoé Gendebien[1], Christophe Poulet[1], Céline Deroyer[1], Geneviève Paulissen[1], Pauline Salpetier[1], Alexandre Hego[2], Gaëtan Lefèvre[2], Gaël Cobraiville[1], Sophie Neuville[1], Zelda Plener[1], Christophe Daniel[3], Thierry Thirion[3], Tatiana Sokolova[4], Patrick Durez[4], Patrice Hemon[5], Yuna Delarue[5], Nadège Marec[5], Elettra Bianchi[6], Philippe Delvenne[6], Clio Ribbens[1] and Dominique de Seny[1]✉

A strong crosstalk exists between endoplasmic reticulum (ER) stress and synovitis. Beyond their canonical role in protein folding, ER stress chaperones may promote inflammation, cell survival, and fibroblast activation under pathological conditions. This study aimed at localizing and quantifying 11 ER stress proteins (BiP, HYOU1, MANF, PDIA4, GANAB, HSP90B1, TXNDC5, DNAJB11, LMAN1, ERP29, CALR) in human inflamed synovial membranes and at investigating their expression in fibroblast-like synoviocytes (FLS) under ER stress, pro-inflammatory, or pro-fibrotic stimuli. By immunohistochemistry, on a first cohort of formalin-fixed paraffin-embedded (FFPE) biopsies obtained from patients with osteoarthritis (OA), chronic pyrophosphate arthropathy (CPPA), and rheumatoid arthritis (RA), these ER chaperones were primarily localized to the lining in low-grade inflammation (Tak <4) and expanded to the sublining under high inflammatory conditions (Tak ≥4), with a widespread distribution in RA. Imaging mass cytometry, applied to a second cohort of FFPE tissue samples collected from patients diagnosed with OA and RA, revealed the co-expression of ER stress proteins with $CD55^+$ FLS in the lining and their progressive infiltration into the sublining along with $CD34^+CD31^-$ FLS during inflammation. These observations were confirmed by immunofluorescence on a larger cohort of OA patients. As inflammation progresses, there is a loss of co-expression with CD55 in the lining, accompanied by a gradual shift towards co-expression with CD34 in the sublining. In vitro, ER stress proteins, particularly BiP, HYOU1, MANF, PDIA4, HSP90B1, LMAN1, CALR, and DNAJB11 are overexpressed in human OA FLS following ER stress, pro-inflammatory or pro-fibrotic stimulation, with BiP, PDIA4, HSP90B1, ERP29, and CALR also being secreted. PDIA4 emerged as a central player: its depletion significantly impaired FLS proliferation and migration, highlighting a direct role in driving synovitis. This study provides the first spatial and functional characterization of ER chaperones in human arthritic synovium, linking ER stress to fibroblast plasticity, inflammation, and fibrosis.

Cell Death & Differentiation; https://doi.org/10.1038/s41418-026-01841-3

INTRODUCTION

The synovial membrane is a connective tissue that surrounds joints and contributes to their homeostasis and lubrication. It is composed of two layers: the lining and sublining. The lining is a thin layer in contact with synovial fluid and contains two synoviocyte types: (i) macrophage-like synoviocytes (MLS, 75%) with phagocytic activity and macrophage markers, and (ii) fibroblast-like synoviocytes (FLS) secreting collagen and hyaluronan. The sublining is less compact and is mainly composed of blood vessels, fibroblasts, and adipocytes, with few resident interstitial macrophages and lymphocytes in a collagenous extracellular matrix [1].

Synovitis is characterized by FLS proliferation and hyperplasia of the lining cells, with immune cell infiltration, neoangiogenesis, and fibrosis. These characteristics appear in both osteoarthritis (OA) and rheumatoid arthritis (RA) but are more pronounced in the latter [1, 2]. Inflammation rapidly alters lining morphology and MLS orientation, abrogating cell–cell contacts [3]. Simultaneously, FLS infiltrate the sublining and differentiate into pro-inflammatory and pro-fibrotic subsets [3, 4]. Single-cell RNA sequencing studies have identified key markers distinguishing FLS subsets in synovial tissue. CD55 marks lining FLS, which are central to synovial fluid production and play a homeostatic role through their barrier function, whereas CD34 characterizes sublining FLS, which exhibit distinct responses to cytokine signaling and express genes linked to fibrosis and angiogenesis in pathological conditions [5–8].

The endoplasmic reticulum (ER) ensures proper protein folding and trafficking through the activation of chaperones. When

[1]Laboratory of Rheumatology, GIGA Research Center, Centre Hospitalier Universitaire de Liège, University of Liège, Liège, Belgium. [2]GIGA Cell Imaging, University of Liège, Liège, Belgium. [3]Orthopedic Surgery Department, Centre Hospitalier Universitaire de Liège, Liège, Belgium. [4]Division of Systemic and Inflammatory Rheumatic Diseases, Institute of Experimental and Clinical Research, Catholic University of Louvain, Brussels, Belgium. [5]LBAI, UMR1227, Univ Brest, Inserm, Brest, France. [6]Department of Pathology, GIGA Research Center, Centre Hospitalier Universitaire de Liège, University of Liège, Liège, Belgium. ✉email: ddeseny@chuliege.be

Received: 29 October 2025 Revised: 13 July 2026 Accepted: 27 July 2026
Published online: 12 August 2026

misfolded proteins accumulate, the unfolded protein response (UPR), involving IRE1, PERK, and ATF6, is triggered to restore homeostasis [9, 10]. Sustained ER stress can promote inflammation via ROS, calcium release, and NF-κB activation [11]. Moreover, chaperones may acquire pro-inflammatory roles when exposed on the cell surface or secreted, enhancing cytokine production and promoting FLS proliferation and migration [12, 13].

Evidence indicates that ER stress pathways are directly implicated in the pathogenesis of synovitis [14–17]. Building on this concept, we recently used mass spectrometry to identify ER stress proteins in synovial membranes from patients with OA, chronic pyrophosphate arthropathy (CPPA), and RA, and exhibiting a continuous degree of inflammation [18]. Expression level of eleven ER stress proteins: BiP (binding immunoglobulin protein), HYOU1 (hypoxia up-regulated 1), MANF (mesencephalic astrocyte-derived neurotrophic factor), PDIA4 (protein disulfide isomerase A4), GANAB (α-subunit of glucosidase II), HSP90B1 (heat shock protein 90 beta family member 1), TXNDC5 (thioredoxin domain containing 5), DNAJB11 (dnaJ heat shock protein family member B11), LMAN1 (lectin mannose- binding 1), ERP29 (endoplasmic reticulum protein 29) and CALR (calreticulin) were strongly correlated to the histological inflammatory score (HIS) based on hyperplasia, macrophages, lymphocytes, plasmocytes and neutrophils infiltration in synovial membranes [18].

In this study, we aimed to characterize the spatial distribution of ER stress proteins within inflamed human synovial membranes and in a mouse model, with a particular focus on $CD55^+$ and $CD34^+$ FLS subpopulations using imaging mass cytometry (IMC) and immunofluorescence (IF) on two distinct cohorts. Moreover, we investigated the potential role of these ER stress proteins in fibroblast proliferation using primary FLS.

This study provides the first spatial characterization of ER stress proteins across distinct fibroblast subpopulations within the synovitis, revealing a dynamic and progressive pattern of expression within $CD55^+$ and $CD34^+$ FLS, which correlates with the inflammatory grades.

METHODS

Synovial biopsies

All experiments were undertaken with patient material complying with the regulations and ethical guidelines of the University Hospital of Liège (CHU) and the Catholic University of Louvain (UCLouvain), Belgium, and were approved by their respective ethical committee (for CHU cohorts- ref: 2017/147, for UCLouvain cohort- ref:2013/24MAI/293) and the biobank research committee (CHU—BB190058, UCLouvain –BB190044). Synovial biopsies were obtained via needle arthroscopy or small joint ultrasonography guided biopsy and were embedded in paraffin for immunohistochemistry (IHC) analysis. Three cohorts (Supplementary Table 1a) were included: (i) cohort 1 ($n = 24$) for IHC from the Center Hospitalo-Universitaire de Liège (CHU Liège) naïve of any treatment [18]; for this cohort, no statistically significant differences were observed between groups for gender, age, or BMI. (ii) cohort 2 from UCLouvain ($n = 3$) used for imaging mass cytometry (IMC); (iii) cohort 3 ($n = 25$) from CHU of Liège for immunofluorescence (IF). For each cohort, chosen biopsies collectively illustrated a continuous inflammatory gradient according to a modified version of the Tak score, modified by excluding vascular parameters (hereafter referred to as "Tak score"—Supplementary Table 1b), which is based on hyperplasia (hy; 0–4 score), lymphocytes (ly; 0–4 score), plasmocytes (pl; 0–4 score), and neutrophils (PMN; 0–3 score) infiltration [19]. Hematoxylin eosin stained sections were scored by anatomopathologists (EB & PD) for each histological feature providing the Tak score. Based on this scoring system, "non-inflammatory (NIN) OA" was defined as OA samples with low Tak scores (Tak <4), while "inflammatory (IN) OA" corresponded to samples with higher Tak scores (Tak ≥4).

Collagenase-induced synovitis mouse model

All animal experimentation procedures were approved by the local ethical committee (LA1610002; #14-1721 University of Liège, Liège, Belgium). The collagenase-induced synovitis (CIS) mouse model was performed as previously described by Deroyer *et al* [20]. Briefly, 8-week-old C57BL6 male mice were anesthetized using isoflurane. Only male mice were used in this study, as OA is known to be more robustly induced in males than in females in experimental models, even though the human tissue cohort primarily consisted of aging women (see Supplementary Table 1a) [21, 22]. Intra-articular injection was performed randomly into knee joint cavities with collagenase VII for CIS generation (1U per articulation, Sigma-Aldrich, St Louis, Michigan, USA) or NaCl 0.9% (control mice) two times, 2 days apart. Mice were sacrificed 1 week later, and joints were collected. Synovial membrane inflammation in CIS mice was confirmed by the overexpression of mRNA *Il1b* and *Il6* measured by RT-qPCR and synovial thickness [20]. Overexpression of *Acta2* mRNA also confirmed the initiation of fibrosis [20]. Investigators were not blinded to group allocation.

Immunohistochemistry analysis

IHC was performed on human and mouse synovial membranes. For human samples, tissues obtained from the ULiège cohort (Cohort 1) were fixed in 4% paraformaldehyde for 24 h (h), then treated in 70% (v/v) ethanol and embedded in paraffin. For mouse samples, the knee joints were fixed in 4% paraformaldehyde for 24 h, followed by decalcification in EDTA for 15 days. They were then dipped in 70% (v/v) ethanol and embedded in paraffin. IHC was then performed on the slide after heating, dewaxing, and antigen retrieval using a steamer for 10 min in target retrieval solution (Agilent, Santa Clara, California, USA). To block endogenous peroxidases and non-specific sites, slides were incubated with hydrogen peroxide and DakoReal antibody diluent (Agilent), respectively. For human FFPE, sections were incubated with a primary antibody (Supplementary Table 2) against chaperone proteins of interest. For mouse model (CIS), only BiP, MANF, PDIA4, HSP90B1, CALR, DNAJB11, and LMAN1 antibodies could be used due to species compatibility. Each ER stress protein is referred to its gene name in Supplementary Table 2. Sections were then incubated with EnVision+System-HRP-labeled polymer (Agilent), and peroxidase was detected using the Liquid DAB+ Substrate Chromogen System (Agilent). Proteins of interest were localized, semi-quantified and normalized for the total number of cells using *QuPath* software [23].

Imaging mass cytometry

Imaging Mass Cytometry™ (IMC™) (Hyperion Imaging System, Standard BioTools™, California) was performed on FFPE tissue provided from 3 patients of the UCLouvain cohort (Cohort 2) as described in the Supplementary Table 1. These tissues were deparaffinized and then treated with antigen retrieval buffers. The sections were incubated with a mixture of metal-conjugated antibodies (Supplementary Table 2) and a DNA intercalating agent for nuclear staining. Each antibody was labeled with a unique metal isotope, allowing for specific recognition of its corresponding antigen and enabling multiplexed spatial protein profiling by imaging mass cytometry (CyTOF). The Hyperion Imaging System (Standard BioTools™, South San Francisco, USA) performed laser desorption of ionized isotopes on selected regions of interest of the synovial tissue. These ions were then separated according to their *m/z* ratio and quantified by the CyTOF instrument, providing information about the intensity and spatial distribution of our proteins of interest.

Multiparametric images obtained by IMC were further studied by the imaging platform (GIGA-Cell Imaging, ULiège). Raw imaging mass cytometry data in ".mcd" format were converted to the standardized ".ome.tiff" format using a custom Python script developed in-house, ensuring the complete preservation of spatial metadata and compatibility with downstream analysis tools. Tissue classification and nuclear segmentation were performed using QuPath (v0.5.1) on the standardized images. Tissue regions were segmented using a pixel classifier trained in QuPath to distinguish tissue from background based on DAPI fluorescence intensity, using a Random Forest algorithm. Nuclei were segmented using StarDist,integrated into QuPath via its dedicated extension. Segmentation was performed on the DAPI fluorescence channel, using a custom-trained StarDist model optimized for histological nuclear features. Using the resulting single-cell masks, Mass Spectrometry signal for 19 markers (Supplementary Table 2) were quantified on a per-cell basis within QuPath. The default threshold for each marker was defined based on the three samples, using the mean plus two standard deviations, after filtering out all cells with values exceeding 1.5 times the interquartile range. Downstream analysis was performed using CytoMAP (v1.4.21). Clustering was conducted using a Self-Organizing Map (SOM) algorithm with *Nearest Neighbor (NN)* spatial context, and the optimal number of clusters was determined using the Davies–Bouldin index.

Immunofluorescence on formalin-fixed paraffin-embedded tissues

Formalin-fixed paraffin-embedded tissue slides from the Cohort 3 (CHU of Liège—25 OA) were incubated overnight at 65 °C. Slides were deparaffinized, followed by antigen retrieval using heat-induced epitope retrieval (HIER) with Target Retrieval Solution (Agilent). Endogenous peroxidase activity was blocked with H_2O_2 for 20 min. To reduce background and begin permeabilization, slides were incubated in a solution of 0.4% Triton X-100 (CAS-9036195; Sigma Aldrich) and 125 mM glycine. Slides were placed in a humidified chamber, and non-specific binding was blocked with Protein Block Serum-Free (Agilent, X0909). Three successive cycles of primary (Supplementary Table 2) and corresponding secondary antibody incubations were performed, each separated by permeabilization and blocking steps. Step 1: mouse anti-CD34 and rabbit anti-PDIA4 (or anti-CALR), followed by anti-mouse Alexa Fluor 594 (ab150116, Abcam) and anti-rabbit Alexa Fluor 532 (A11009, Thermo Fisher). Step 2: rabbit anti-CD55 followed by anti-rabbit Alexa Fluor 488 (ab150081, Abcam). Step 3: directly conjugated antibodies anti-CD68-Alexa Fluor 647 and anti-CD31-Alexa Fluor 750. On day 4, nuclear staining was performed with DAPI (1:1000) for 30 min. Slides were mounted with ProLong Diamond Antifade Mountant and stored at 4 °C. Image acquisition was performed using a Leica Stellaris 8 confocal imaging system and proteins of interest were next localized and semi-quantified using *QuPath* software [23].

Cell culture and treatment

Synovial tissues were obtained prospectively by orthopedic surgeons of the CHU Liège from patients who underwent prosthetic surgery for knee OA. The research ethics committee of our hospital, CHU of Liège, Belgium, approved the study (ref: 2023/4). To isolate human FLS from synovial membrane, the tissue was digested with collagenase overnight at 37 °C. Cells were filtrated and resuspended in DMEM containing 10% fetal bovine serum (FBS). Cells were used between passages 3 and 7. Synovial membranes used for FLS isolation were provided from 60 patients: 45% females and 55% males with a median age of 67 (54–84) years and a median BMI of 34.5 (19.05–38.27) kg/m^2. ER stress was induced by tunicamycin (Tm; 1ug/mL; Sigma Aldrich) for 1, 3, or 7 days before supernatant and protein extract collection. For protein secretion in supernatants, FBS 1% was used instead of FBS 10%. Inflammation was induced by TNF-α (10 ng/mL, Peprotech, London, UK) for 1, 3, or 7 days. Pro-fibrotic response was induced by TGF-ß (10 ng/mL; ThermoFischer) for 1, 3, or 7 days. Cell extracts and supernatants were then collected. These stimulation time points were defined based on preliminary data from our laboratory on OA FLS [24, 25] and supported by the literature, showing time-dependent induction of ER stress markers [26], pro-inflammatory cytokines (e.g., IL-1β, IL-6) [24, 27], and pro-fibrotic markers (e.g., αSMA, fibronectin) [24, 25]. The UPR pharmacological inhibitors (MedChemExpress) of IRE1α (4μ8C, 100 μM; HY-19707), PERK (PERK-IN-2, 0.01 μM; HY-135220) or ATF6 (Ceapin-A7, 0.5 μM; HY-108434) were applied 4 h before a 1-day or 3-day stimulation with Tm or TGF-ß, respectively. Diméthylsulfoxyde (DMSO) was used on controls. Protein extracts were collected for downstream analysis.

Immunofluorescence on fibroblast-like synoviocytes (FLS)

FLS were seeded on glass coverslips, stimulated by Tm (1 μg/mL) for 3 days, and fixed with 4% paraformaldehyde for 10 min. Cells were then permeabilized and blocked using PBS supplemented with 1% BSA, 5% FBS, and 0.1% Triton X-100 for 30 min. Cells were then incubated overnight at 4 °C with primary antibodies against CD55 or CD34 (Supplementary Table 2). Coverslips were incubated for 1 h with an Alexa Fluor 647-conjugated anti-rabbit secondary antibody (A-21235; Invitrogen). Nuclei were counterstained with DAPI (1:1000), and coverslips were mounted using ProLong Gold Antifade Mountant.

siRNA transfection

For RNA interference, the decreased expression level of HYOU1 (s20632), MANF (s15436), PDIA4 (s225164), DNAJB11 (s28581), or CALR (s115) was obtained by siRNA transfection (Life Technologies) using Lipofectamine™ 2000 (Thermo Fisher Scientific, Cat. No. 11668030). siRNAs were resuspended to 100 μM stock solutions and diluted to 10 μM working solutions. For transfection, siRNAs were diluted either 1:10 (HYOU1, DNAJB11) or 1:20 (MANF, PDIA4, CALR) in Opti-MEM™, while Lipofectamine™ 2000 was diluted 1:50 in Opti-MEM™, using equal volumes. After 5 min incubation at room temperature (RT), both solutions were mixed and incubated for 15 min to allow complex formation. The transfection mix was then added dropwise to the cells, resulting in a final 1:10 dilution in the culture medium. A Negative Control siRNA (siCtrl, Cat. No. 4390843) was used at matching concentrations for each condition, with separate controls corresponding to the 1:10 and 1:20 siRNA dilutions. FLS were seeded in 96-well plates and transfected for 24 h prior to a 3-day TGF-β stimulation.

Viability and proliferation assays

FLS were transfected with siRNAs targeting HYOU1, MANF, PDIA4, DNAJB11, CALR or siCtrl, and were subsequently stimulated with TGF-β for 3 days. Cell viability was evaluated using the MTS assay (Promega, Madison, WI, USA), while cell proliferation was assessed using the BrdU incorporation assay (Abcam), following the manufacturers' instructions. Results are expressed as the percentage of viable (MTS assay) or proliferating (BrdU assay) cells. Proliferation and MTS assays were performed separately for HYOU1 and DNAJB11 on the one hand, and for MANF, PDIA4, and CALR on the other, as each protein group was compared with its own matched control condition at the corresponding concentration. Accordingly, their respective depletions were carried out and quantified in parallel but analyzed independently.

Migration assay

OA FLS were seeded in both 96-well plates (for migration analysis) and 24-well plates (for validation of PDIA4 depletion) and cultured in DMEM supplemented with 10% FBS until reaching full confluence. Three days post-seeding, the culture medium was replaced with low-serum medium (0.5% FBS), and cells were transfected in the morning with either control siRNA (siCtrl) or siRNA targeting PDIA4 (siPDIA4). Six hours later, cells were stimulated or not with TGF-β. For migration analysis, 96-well plates were processed using the IncuCyte Live-Cell Analysis System. Wound areas were defined using the IncuCyte plate map editor, and cell migration was monitored in real time over a period of 60 h. Images were acquired automatically, and relative wound density (RWD) was quantified over time. Experiments were terminated after the 60 h acquisition period. In parallel, cells cultured in 24-well plates were harvested for protein extraction to confirm the efficiency of PDIA4 knockdown by Western blot analysis.

Western blotting

FLS were lysed in RIPA buffer. Proteins from cell lysates were then separated onto polyacrylamide gels. Proteins were then transferred overnight on polyvinylidene difluoride membranes (Millipore, Tullagreen, Ireland), which were further blocked with 10% milk for 1 h at RT. The blots were first incubated with the primary antibody (Supplementary Table 2) for 3 h at RT, washed, and then incubated with the horseradish secondary antibodies (anti-mouse or anti-rabbit; Cell Signaling Technology) for 45 min at RT. Proteins of interest were detected by chemiluminescent detection solution (ECL Western blotting substrate; Thermo Scientific, Rockford, USA). Glyceraldehyde-3-phosphate dehydrogenase (anti-GAPDH #G9545; Sigma) and Heat Shock Protein (anti-HSP90 #13171-1-AP; Proteintech) were used as protein-loading controls for intracellular extracts, whereas Ponceau S stain (CAS-6226795; Sigma Aldrich) was used for supernatants. Intensities were normalized using the corresponding loading control and further quantified using ImageJ software (version 1.53).

RT-qPCR

Total RNA was extracted using the NucleoSpin RNA kit (Macherey–Nagel, Düren, Germany). RNA was reverse-transcribed using the RevertAid H Minus First Strand cDNA Synthesis Kit (Thermo Fisher Scientific, USA). cDNA was amplified by real-time PCR using the KAPA SYBR FAST system (Sopachem, Belgium) on a LightCycler 480 instrument (Roche Diagnostics, Germany). PCR efficiency $E = 10^{(-1/\text{slope})}$ was determined for each primer using standard curves generated from serial cDNA dilutions. Relative gene expression was calculated using the $2^{-\Delta CT}$ method, with untreated samples used as calibrators and GAPDH as the econtrol. Primers were purchased from Integrated DNA Technologies (IDT) (Supplementary Table 2).

Statistics

Data were analysed with Prism™ software (v9.3.1, GraphPad, Boston, USA) and were considered statistically significant when p values were <0.05 (*$p < 0.05$, **$p < 0.01$, ***$p < 0.001$, ****$p < 0.0001$). The Kolmogorov–Smirnov

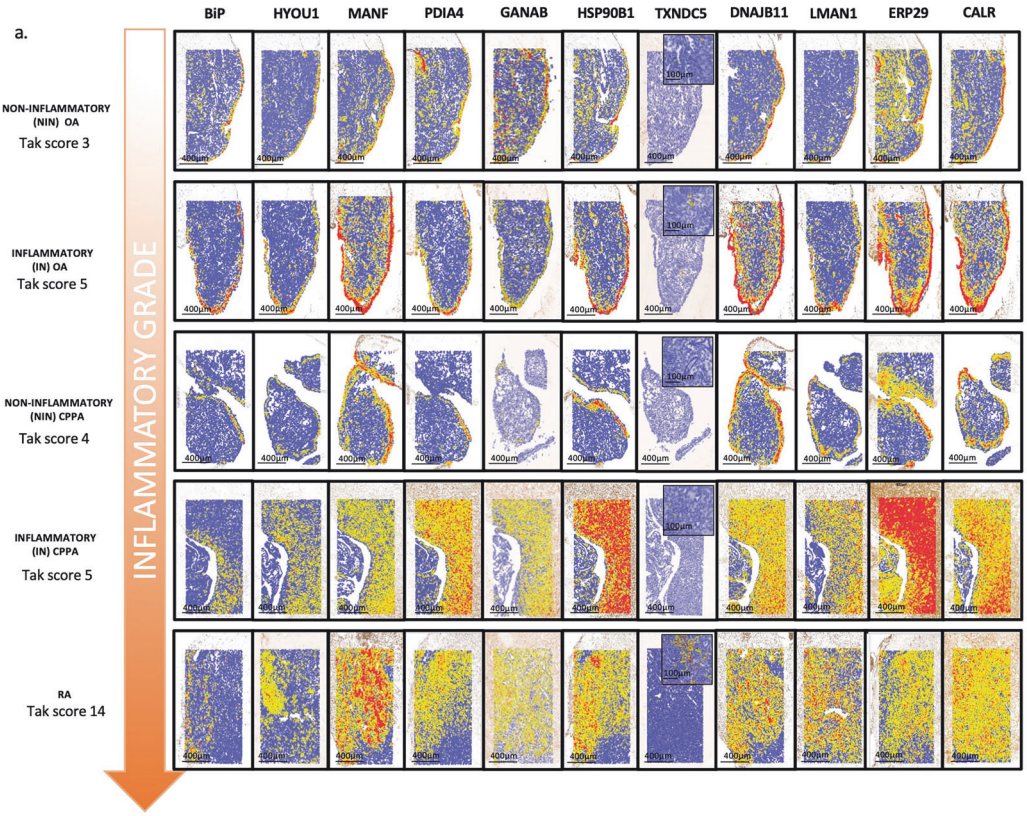

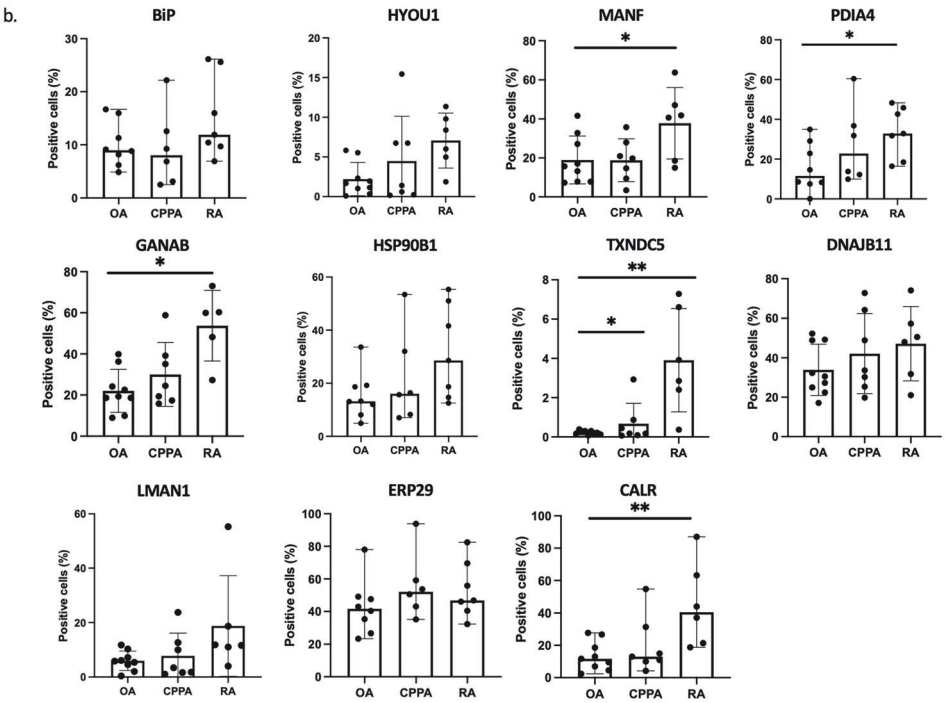

test was used to assess the distribution. For values that passed the normality test, parametric tests were applied: a paired *t* test for two-group comparisons and a paired ANOVA test followed by a Tukey post hoc test for multiple comparisons. For values that did not pass the normality test, nonparametric tests were used. For paired data, the Wilcoxon signed-rank test (two groups) or the Friedman test (more than two groups), followed by Dunn's post hoc test with appropriate correction for multiple comparisons, was applied. For unpaired data, the Kruskal–Wallis test followed by Dunn's post hoc test was used for multiple group comparisons. Migration data were analyzed using linear mixed-effects models to account for repeated measures. Treatment condition, time, and their interaction were included as fixed effects, with patient as a random effect. Analyses were performed in R using the lme4 and

Fig. 1 Localization of the 11 ER stress proteins in synovial membranes provided from patients with osteoarthritis (OA), chronic pyrophosphate arthropathy (CPPA) and rheumatoid arthritis (RA). a Immunohistochemistry illustrations of the 11 ER stress proteins of interest provided from FFPE synovial membranes of OA ($n \geq 8$), CPPA ($n \geq 6$), and RA ($n \geq 5$) patients (Cohort 1); and **b** their quantification (optical density values) obtained by QuPath. Highly positive cells have an OD > 0.6 (red spot), moderately positive 0.4 > OD > 0.6 (orange spot), weakly positive 0.2 > OD > 0.4 (yellow spot), and negative cells <0.2 (blue spot). Data were analyzed with Prism 9 software (GraphPad). Graphs illustrate the median with a 95% confidence interval of the data. Statistical differences were considered for p values < 0.05 (*$p < 0.05$, **$p < 0.01$, ***$p < 0.001$). Statistical analysis was performed using the nonparametric unpaired Kruskal- Wallis test followed by Dunn's post hoc test for multiple comparisons. Each point represents one biopsy (one patient), and n indicates the number of independent biopsies. ER endoplasmic reticulum, NIN non-inflammatory, IN inflammatory and OD optical density.

ImerTest packages. Model assumptions were verified by inspection of residuals, including normality, homoscedasticity, and linearity over time. Effect sizes were calculated according to Cohen.

RESULTS

Localization and quantification of ER stress proteins in inflamed human and mouse synovial membranes

Following our previous proteomic analysis providing bulk protein expression [18], ER stress proteins were detected by IHC on synovial biopsies from the same patients. BiP, HYOU1, MANF, PDIA4, GANAB, HSP90B1, TXNDC5, DNAJB11, LMAN1, ERP29, CALR were detected, though TXNDC5 remained consistently low. In mildly inflamed tissues (Tak <4), expression restrained to the lining layer, while in highly inflamed samples (Tak ≥4), proteins extended into the sublining (Fig. 1a). In the quantification, MANF, PDIA4, GANAB, TXNDC5, and CALR were significantly overexpressed in RA (Fig. 1b). Differences for BiP, HYOU1, HSP90B1, DNAJB11, and LMAN1 were not statistically significant, likely due to overlapping Tak scores (Supplementary Fig. 1). Differential expression exists in positive cells between non-inflammatory (NIN) and inflammatory (IN) conditions in OA and CPPA for MANF, PDIA4, HSP90B1, DNAJB11, ERP29 and CALR (Supplementary Fig. 1).

Imaging mass cytometry, performed on the second cohort illustrates the same pattern of ER stress protein infiltration into the sublining as inflammation progresses (in NIN OA, IN OA, and RA–Fig. 2a). As shown in Fig. 2a, their expression was restricted to the lining in Tak 0, observed predominantly in the sublining in Tak 4, and extended to the whole synovium in Tak 13. This is further supported by a semi-supervised clustering analysis expressed as fold change, calculated as the ratio of each chaperone's expression in a given region to its average across all the regions in the three biopsies. Four distinct clusters (regions 1 to 4, color-coded) emerged based on the mean expression of ER stress proteins. Column values represent the mean fold change across all chaperones, revealing a gradient from low expression in region 1 (blue) to high expression in region 4 (orange) (Fig. 2b). In Fig. 2c, the low-expression blue region (or blue column) is predominantly located in the sublining independently of the inflammatory status. By contrast, the intermediate-expression yellow region (or beige column) is mainly present in the lining in both NIN and IN OA, while the highest-expression orange region (red column), of particular interest, infiltrates the sublining as inflammation advances. All the regions extend throughout the synovium in RA (Fig. 2c).

IHC analysis in CIS mouse model confirmed increased expression of six chaperones (MANF, PDIA4, HSP90B1, DNAJB11, LMAN1, and CALR,) in inflamed synovium compared to controls (Supplementary Fig. 2a-b). MANF, LMAN1, and DNAJB11 showed a positive correlation with pro-inflammatory cytokines (*Il1b* and/or *Il6*); PDIA4, HSP90B1, and CALR with the fibrotic marker *Acta2*; and MANF, HSP90B1, DNAJB11, LMAN1, and CALR with synovial thickness (Supplementary Fig. 2c).

Targeting and localizing synovial cells of interest within the human inflamed synovial membranes

Based on the progression of expression and infiltration of ER stress proteins, we aimed to investigate which synovial cellular markers, among all the data obtained by the IMC™, exhibited similar patterns. Computational analysis identified potential cell subpopulations expressing these proteins, with 3 markers that stood out from our analysis: CD55 (lining FLS), CD34 (sublining FLS) and CD68 (MLS) (Fig. 3a). Sublining FLS were distinguished from endothelial cells by the exclusion of CD31 marker ($CD34^+CD31^-$). Illustrated by red dots (high protein level expression), CD55 showed a strong expression in the lining layer of OA but completely disappeared in RA. In contrast, CD34, was primarily found in the sublining layer of inflamed OA but less in the lining as observed with NIN OA. CD34 was present throughout the synovial tissue in RA, which had lost its typical architecture. CD68 exhibited a similar expression pattern to CD55 but remained in RA tissues (Fig. 3a). Both $CD3^+$, $CD4^+$ T cells, and $CD20^+$ B cells were present within the lymphoid infiltrates in both NIN and IN OA, while in RA, these lymphocytes were more diffusely distributed throughout the synovial tissue (Fig. 3b).

Co-expression of ER stress proteins with fibroblast-like synoviocytes

Based on our initial investigations of the localizations of ER stress proteins and synovial cells ($CD55^+$, $CD34^+CD31^-$, and $CD68^+$), we sought to determine, whether these ER stress proteins were co-expressed with one of these cell specific subpopulations. IMC™ approach aimed to identify potential interactions or relationships between these proteins and specific cell types within the synovial membrane. As ER stress proteins co-expressed with each other (Supplementary Fig. 3), PDIA4 was selected for clarity to represent the entire set of chaperone proteins (Fig. 4a). In the NIN OA, ER stress proteins are predominantly localized in the lining layer. In this compartment, they co-expressed with $CD55^+$ FLS and with $CD68^+$ MLS, while $CD34^+CD31^-$ FLS are nearly absent. In the IN OA, ER stress proteins infiltrate the sublining and co-expressed with $CD34^+CD31^-$ FLS, while CD55 and CD68 expression remain confined to the lining (more abundant for CD55). In RA, the synovial architecture is disrupted. CD55 expression is lost, whereas CD34, CD68, and chaperones are widely distributed throughout the synovial tissue (Fig. 4a). For lymphocyte markers (CD3, CD4, and CD20), both in NIN OA and IN OA, their expression was predominantly confined to lymphoid nodules, spatially distinct from the areas where ER stress proteins were detected. CD4 expression was also observed in the lining regardless of the inflammatory status, likely reflecting CD4 expression by macrophages themselves [28, 29] (Fig. 4a). In RA, these markers are widespread within the whole synovium, especially for CD3 and CD4 (Fig. 4a).

The co-expression patterns were confirmed by a supervised clustering analysis of all ER stress proteins within each cellular marker population. This analysis identified two distinct clusters: (i) low co-expression (low fold change) in the blue column representing the green region; and (ii) high co-expression (high fold change) in the red column representing the blue region (Fig. 4b). This latter region (blue region/ red column) was predominantly associated with $CD55^+$ and $CD68^+$ cells in the lining layer of NIN OA (Fig. 4c). In contrast, under inflammatory conditions (Tak ≥4), most ER stress proteins shifted toward the sublining and co-expressed primarily with $CD34^+CD31^-$ fibroblasts, as illustrated by the spatial representation of supervised clustering analysis (Fig. 4c).

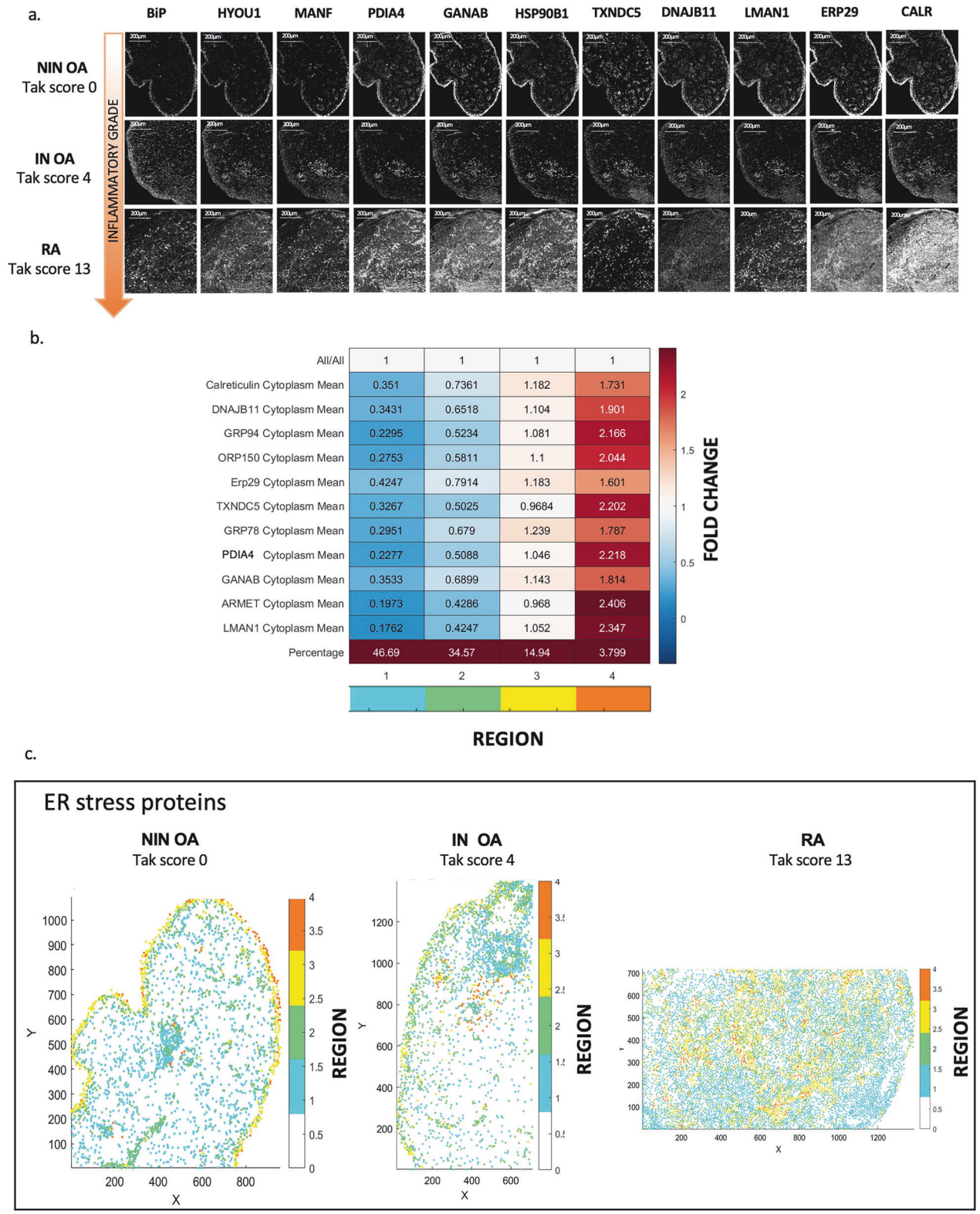

Fig. 2 Spatial distribution and clustering of ER stress protein expression in synovial tissue. a Representative multiparametric imaging mass cytometry (IMC) of synovial sections from patients with OA and RA (Cohort 2, $n = 3$) showing localization of ER stress proteins. One NIN, one IN OA and one RA are selected across the 6 biopsies to represent the inflammatory continuum. **b** Semi-supervised clustering of the 11 ER stress proteins reveals four distinct tissue regions based on protein expression patterns. **c** Map of the semi-clustering by IMC of ER stress proteins in the same biopsies, represented by the four code-colored regions. The region 4 (orange) is defined by high expression level of ER stress proteins. ER endoplasmic reticulum, NIN non-inflammatory, IN inflammatory, OA osteoarthritis, RA rheumatoid arthritis.

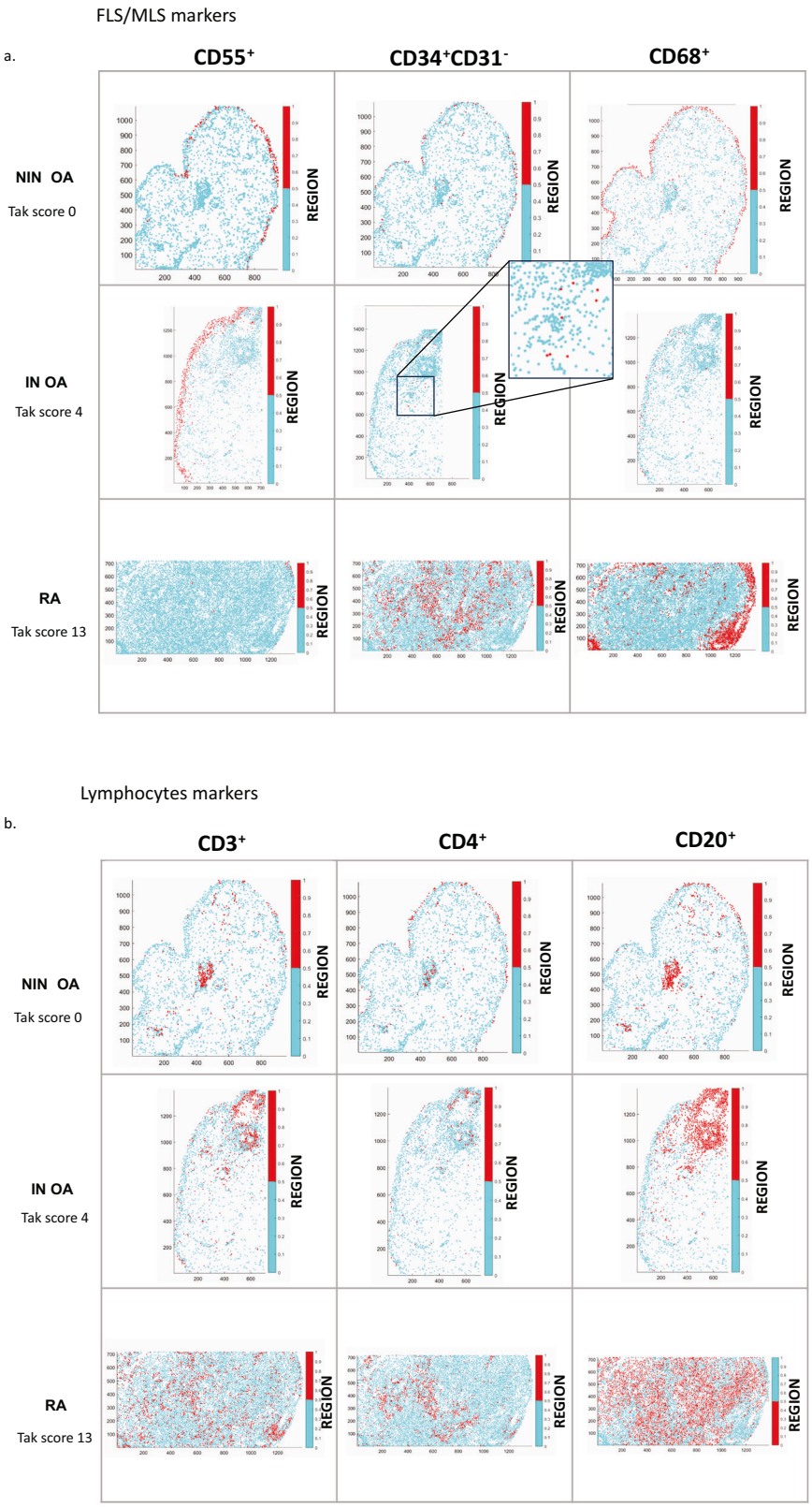

Fig. 3 Spatial mapping of synovial immune and stromal cell subsets in osteoarthritis and rheumatoid arthritis. Spatial representation of supervised clustering analysis of (**a**) synovial fibroblast ($CD55^+$ and $CD34^+$) and macrophage ($CD68^+$) subsets; and **b** T ($CD3^+$ and $CD4^+$) and B ($CD20^+$) lymphocytes in non-inflammatory OA, inflammatory OA, and RA. Red and blue dots, respectively indicate areas with high or no expression of fibroblast, macrophage, T or B cell markers, as defined by the clustering algorithm. NIN non-inflammatory, IN inflammatory, OA osteoarthritis, RA rheumatoid arthritis.

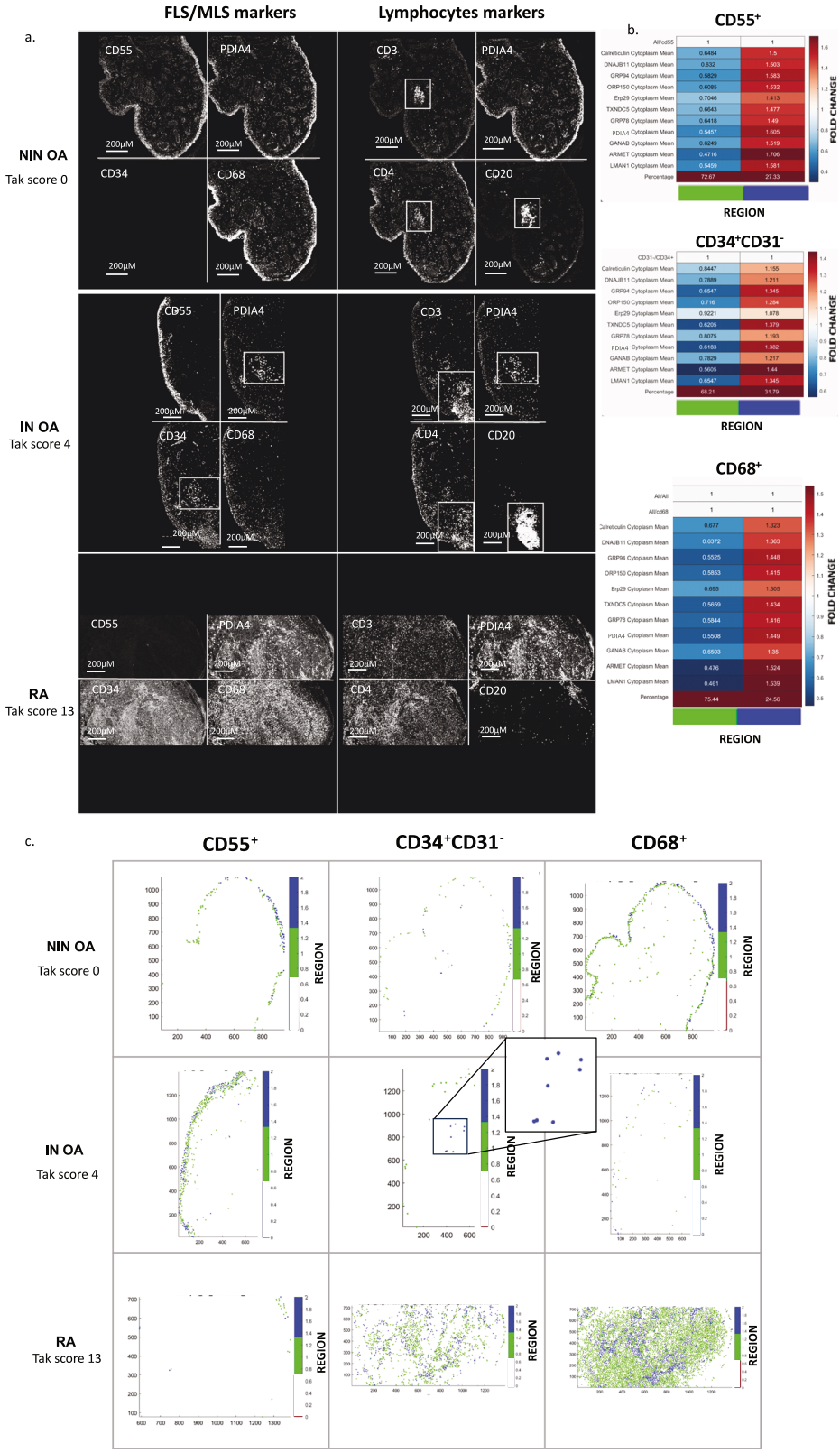

Fig. 4 Co-expression of PDIA4 with FLS in the synovial membrane. a Multiparametric imaging mass cytometry (Cohort 2, $n = 3$) of PDIA4, FLS/MLS and lymphocyte markers. White squares enclose marker infiltration. **b** Supervised clustering analysis of ER stress protein expression within CD55⁺, CD68⁺, and CD34⁺CD31⁻ cell populations. **c** Spatial representation of supervised clustering analysis of ER stress protein co-expression with synovial fibroblast and macrophage subsets in NI OA, IN OA, and RA. Blue dots indicate areas with high co-expression of ER stress proteins with the cell marker, as defined by the clustering algorithm, while green and white areas correspond to regions with lower co-expression. ER endoplasmic reticulum, FLS fibroblast-like synoviocytes, MLS macrophage-like synoviocytes, NIN non-inflammatory, IN inflammatory, OA osteoarthritis, RA rheumatoid arthritis.

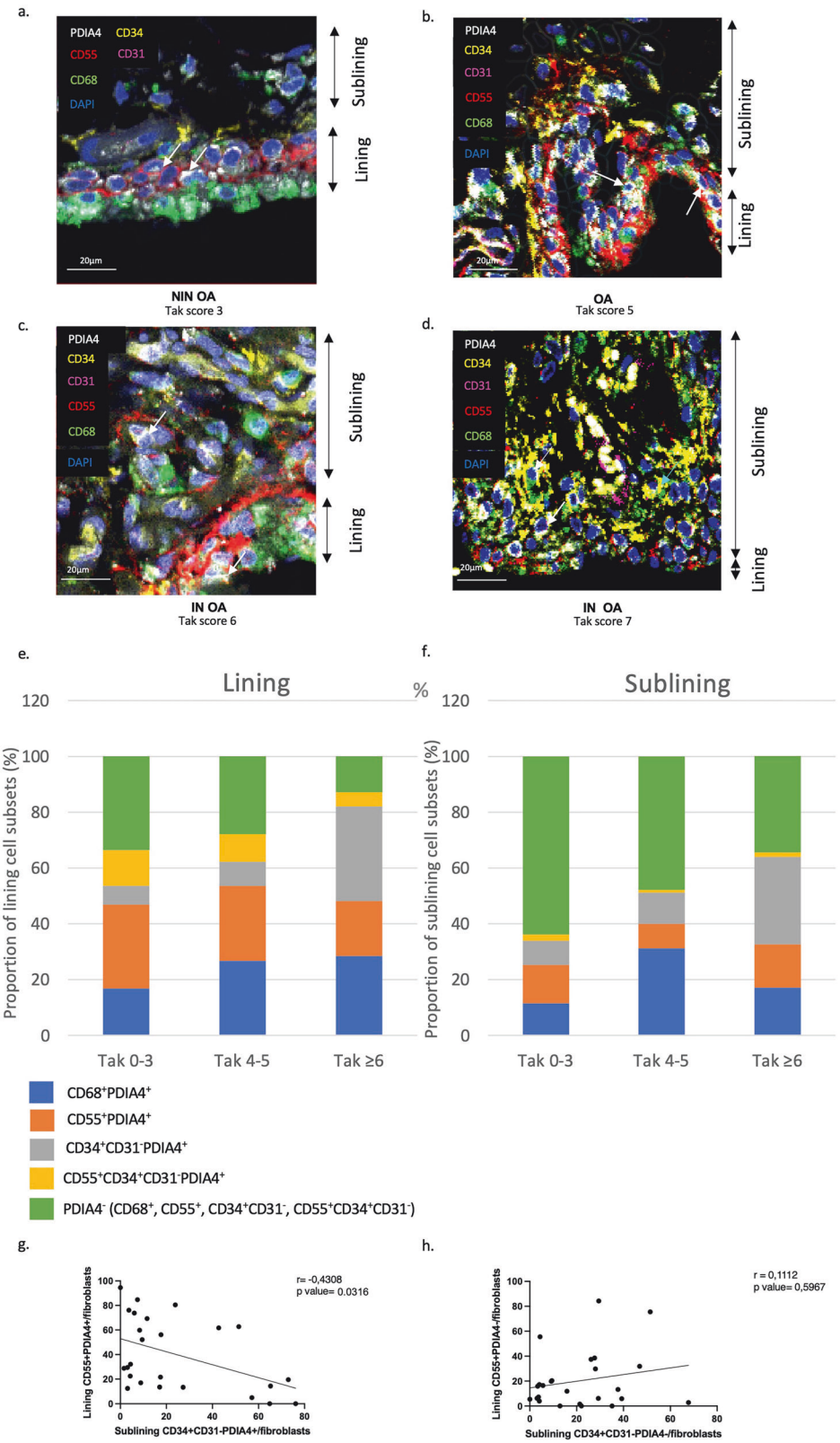

Confirmation of ER stress protein co-expression with FLS on a larger cohort using immunofluorescence

These co-expression patterns were validated in an extended cohort of 25 OA patients using IF (Cohort 3- CHU Liège). First, co-expression of the ER stress protein PDIA4 with FLS markers was confirmed through the detection of their respective fluorescence signals (Fig. 5a–d).

In NIN OA (Tak 3), there was a strong co-expression of ER stress proteins, represented by PDIA4, with $CD55^+$ and $CD68^+$ cells within a well-preserved lining layer (Fig. 5a). This co-expression

Fig. 5 Validation of ER stress protein co-expression with FLS in an extended OA cohort (Cohort 3, $n = 25$) and their transitional phenotypic shift. Immunofluorescence analysis of PDIA4 (white), CD55⁺ (red), CD68⁺ (green) CD34⁺ (yellow), CD31⁺ (pink), and DAPI (blue) in (**a**) non inflamed (Tak 3), **b** intermediate grade (Tak 5), **c** inflamed (Tak 6) and **d** inflamed (Tak 7) OA synovial samples. White arrows show expression of PDIA4 within $CD55^+$, $CD68^+$, or $CD34^+CD31^-$ cells. Panels showing the proportion of $CD68^+$, $CD55^+$, $CD34^+CD31^-$, or $CD55^+CD34^+CD31^-$ cells expressing PDIA4 among total $CD68^+$, $CD55^+$, $CD34^+CD31^-$, or $CD55^+CD34^+CD31^-$ cells in the lining (**e**) and sublining (**f**), stratified by Tak score. **g**, **h** Spearman analysis representing the correlation between CD55⁺ FLS in the lining and $CD34^+CD31^-$ FLS in the sublining, either expressing PDIA4 (**g**) or not expressing PDIA4 (**h**), with increasing Tak scores. A linear regression illustrates this inverse relationship. n = number of independent biopsies (one biopsy per patient). ER endoplasmic reticulum, FLS fibroblast-like synoviocytes, OA osteoarthritis, NIN non-inflammatory, IN inflammatory.

was still evident at an intermediate inflammatory grade (Tak 5) (Fig. 5b). When inflammation worsens, the pattern shifts: at Tak score 6, a weak PDIA4 co-expression with CD55⁺ and CD68⁺ cells persists in the lining, but PDIA4 has already infiltrated the sublining and now co-expresses with $CD34^+CD31^-$ FLS (Fig. 5c). At a higher inflammatory level (Tak 7), the lining is almost erased and the sublining is dominated by $CD34^+CD31^-PDIA4^+$ FLS (Fig. 5d).

Second, a quantitative phenotypic distribution analysis was performed on the lining and sublining, depending on the inflammatory gradient (Fig. 5e-f). For CD55 (orange), in the lining (Fig. 5e), proportion of $CD55^+PDIA4^+$ cells was higher in NIN OA (Tak ≤3, 30%) and decreased in IN OA (Tak >6, 20%), while in the sublining (Fig. 5f), it remained low and stable (14% vs 15%). For CD68 (dark blue), the proportion of $CD68^+PDIA4^+$ cells increased with inflammation, from 17 to 28% in the lining and from 11% to 17% in the sublining. Of interest, for $CD34^+CD31^-$ (gray), the proportion of $CD34^+CD31^-PDIA4^+$ cells markedly increased with inflammation, from 7 to 34% in the lining and from 9% to 31% in the sublining (Fig. 5e, f). Among these, $CD34^+CD31^-$ fibroblasts represent the predominant $PDIA4^+$ subpopulation in both the lining (34%) and sublining (31%) compartments under inflammatory conditions. Proportion of $PDIA4^-$ cells ($CD68^+PDIA4^-$, $CD55^+PDIA4^-$, $CD34^+CD31^-PDIA4^-$, $CD55^+CD34^+CD31^-PDIA4^-$ cells; green), in the lining and sublining progressively diminished with inflammation; in the sublining, it ranged from 64% in NIN OA to 34% in IN OA. These results indicate a redistribution of PDIA4 expression across cell types, with $CD34^+CD31^-$ fibroblasts emerging as the main contributors to the $PDIA4^+$ pool under inflammatory conditions. These findings were validated using another ER stress protein, CALR, following the same experimental approach, including representative staining (Supplementary Fig. 4a–d) across increasing Tak scores and quantitative analyses in the lining (e) and sublining (f). Both qualitative and quantitative analyses confirmed that with increasing inflammation, the proportion of $CD34^+CD31^-CALR^+$ cells increases, whereas $CD55^+CALR^+$ and $CD68^+CALR^+$ populations decrease (Supplementary Fig. 4).

We then sought to determine whether CD55⁺ and CD34⁺ cells represent two distinct populations within the synovial membrane, or whether CD34⁺ cells might rather arise from a transition of CD55⁺ cells toward a CD34⁺ phenotype. Interestingly, we identified the presence of a $CD55^+CD34^+CD31^-$ population (yellow) through co-staining (Fig. 5e, f). Additionally, a negative correlation (Spearman, r = –0.43, *P* value: 0.03) was observed between $CD55^+PDIA4^+$ cells in the lining and $CD34^+CD31^-PDIA4^+$ cells in the sublining across increasing Tak scores, whereas there was no correlation if these fibroblasts did not express this protein (Fig. 5g, h, respectively). This suggests that PDIA4 may be involved in the progressive transition between the two fibroblast populations located in the lining and sublining layers.

ER stress, inflammation and pro-fibrotic conditions modulate chaperone expression and secretion in OA FLS through differential UPR pathway regulation

To investigate ER stress protein regulation in OA FLS, we first confirmed CD55 and CD34 expression by IF and WB (Supplementary Fig. 5a and b, respectively). Both markers were present at baseline and remained unchanged upon ER stress (tunicamycin), or inflammatory (TNF-α) stimulation (Supplementary Fig. 5b). FLS treated with tunicamycin for 1, 3, or 7 days showed significant induction of BiP, HYOU1, MANF, PDIA4, HSP90B1, LMAN1, and CALR (Fig. 6a, b), while GANAB, TXNDC5, DNAJB11, and ERP29 were not modulated (quantification not shown). Most proteins (except BiP) were already detectable at baseline. We then assessed their secretion. BiP, PDIA4, HSP90B1, ERP29, and CALR were secreted after prolonged tunicamycin exposure (Fig. 6c, d). While only PDIA4 was detectable in unstimulated supernatants, ERP29 secretion occurred exclusively at day 7. HYOU1, MANF, GANAB, TXNDC5, DNAJB11, and LMAN1 were not secreted under any condition (data not shown). Under inflammatory stimulation (TNF-α), BiP was overexpressed at day 1, while HYOU1, MANF, and PDIA4 increased at day 3 (Fig. 6e, f). TGF-β stimulation led to elevated BiP at days 1 and 3, and increased HYOU1, MANF, and DNAJB11 expressions at day 3 (Fig. 6g, h). Quantifications are not shown for proteins that were not modulated by TNF-α and/or TGF-β.

Altogether, five proteins—HYOU1, MANF, PDIA4, DNAJB11, and CALR—were consistently modulated by ER stress, inflammatory, or pro-fibrotic stimulation (Supplementary Table 3). They were therefore selected for further investigation as potential regulators of synovial fibroblast activation. To identify the signaling pathways involved in their regulation, cells were pretreated with selective inhibitors of the three canonical UPR branches—IRE1α (4μ8c), PERK (PERK-IN-2), and ATF6 (Ceapin-A7) (Fig. 7). Inhibitor efficacy was confirmed by reduced IRE1α and EIF2α phosphorylation, and decreased ATF6 cleavage (Fig. 7). Accordingly, HYOU1 expression was regulated by both IRE1α (Fig. 7a, b) and ATF6 (Fig. 7e, f), and PDIA4 specifically by ATF6 (Fig. 7e, f). PERK inhibition did not modulate any chaperone expression (Fig. 7c, d). In line with this, inhibition of IRE1α (Supplementary Fig. 6a-b) and, to a lesser extent, inhibition of PERK (c-d) reduced αSMA expression, further supporting a role for UPR signaling in the regulation of pro-fibrotic pathways in OA FLS, whereas ATF6 inhibition had no effect (e-f).

PDIA4 drives proliferation and migration of OA FLS via TGF-β signaling

To assess proliferation and migration, FLS were transfected with siRNAs designed to silence the expression of the genes encoding these five proteins prior to stimulation with TGF-β for 3 days (Supplementary Figs. 7a–d). Proliferation was significantly increased in control cells upon TGF-β stimulation (Fig. 8a). This response was dependent on PDIA4, as PDIA4 silencing under TGF-β stimulation significantly reduced proliferation compared with control siRNA-treated cells (siCtrl + TGF-β vs. siPDIA4 + TGF-β, highlighted in bold). Of note, silencing HYOU1, PDIA4, DNAJB11, MANF or CALR did not affect cell viability (Fig. 8b). These findings suggest that PDIA4 appears to be involved in proliferative processes within the synovium. This is supported by its co-expression with the proliferation marker Ki67 by IMC, with semi-supervised clustering identifying three co-expression levels (cyan: low, green: intermediate, dark blue: high) (Supplementary Fig. 8a), and by spatial mapping revealing

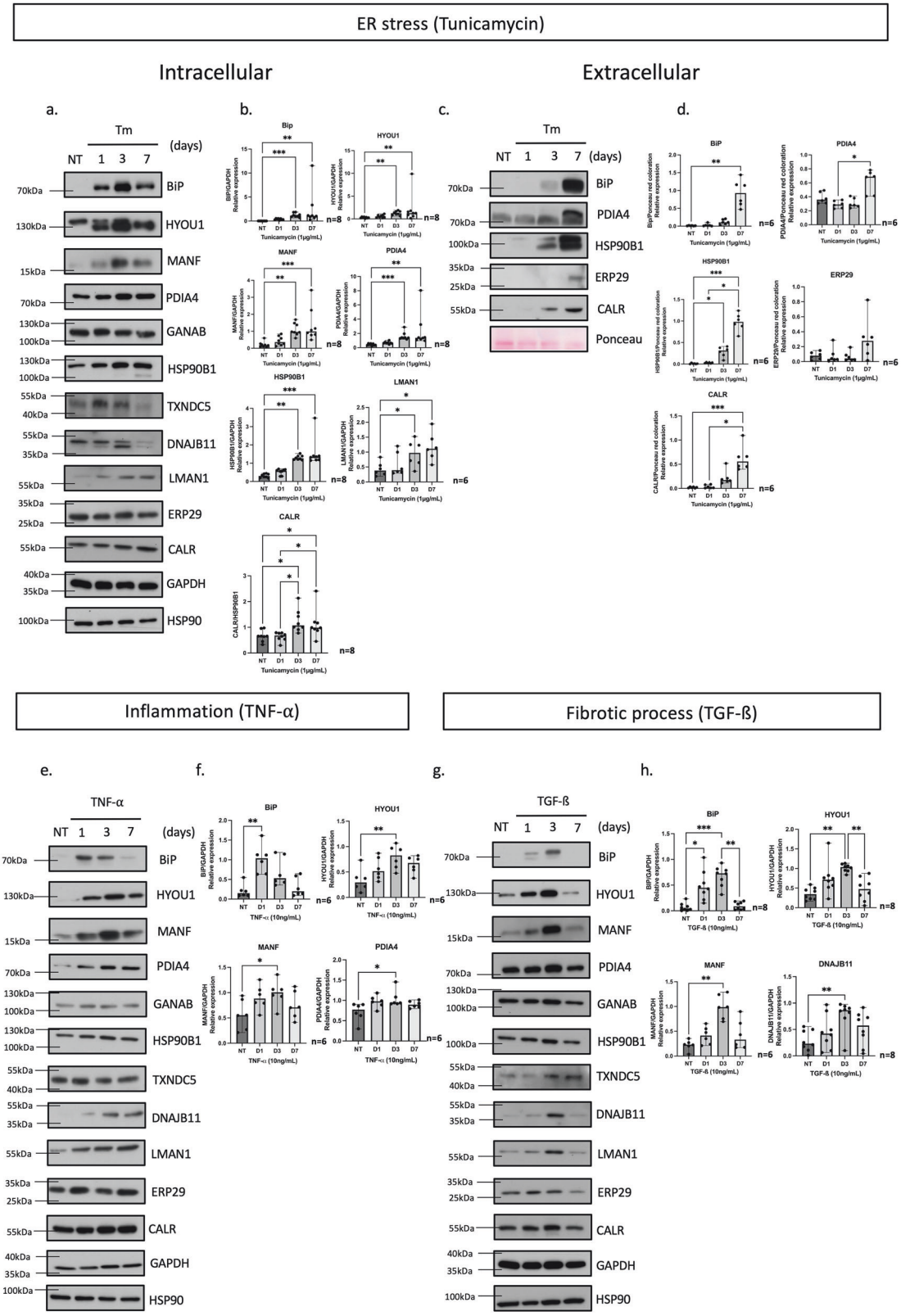

intermediate co-expression in the lining of NIN OA, strong sublining co-expression in IN OA, and a diffuse pattern in RA (Supplementary Fig. 8b).

We next investigated whether PDIA4 also contributes to FLS migration. As expected, TGF-β induced migration in a time-dependent manner, with no significant effect at early time points and a progressive increase thereafter (Fig. 8c). Importantly, PDIA4 silencing reduced TGF-β-induced migration at later stages compared to control conditions, indicating that PDIA4 may promote the pro-migratory response of OA FLS (Fig. 8c).

Fig. 6 Modulation of ER stress proteins after induction of ER stress, pro-inflammatory and pro-fibrotic process. Illustrative Western blot images depicting 11 ER stress proteins intracellular expression following 1, 3 and 7 days of (**a**) Tm (1 µg/mL), **e** TNF-α (10 ng/mL), or **g** TGF-β (10 ng/mL) stimulation on FLS and their respective semi-quantifications (**b**, **f**, **h**). HSP90 or GAPDH expression were used as loading controls. Protein expression and secretion were assessed in parallel by analyzing both intracellular extracts (**a**, **b**) and matched extracellular supernatants following tunicamycin treatment (**c**, **d**). Ponceau S staining served as a protein-loading control. $n \geq 6$. Statistical analysis was performed using the nonparametric paired Friedman test followed by Dunn's post hoc test for multiple comparisons. Only statistically significant quantifications are illustrated. Statistical differences were considered for p values < 0.05 (*$p < 0.05$, **$p < 0.01$, ***$p < 0.001$). Data are presented as median with 95% CI. Each point represents one measurement obtained from an individual patient under a specific stimulation condition. n indicates the number of independent patients. NT non-treated, D day. ER endoplasmic reticulum, Tm tunicamycin, TNF-α tumor necrosis factor-α, TGF-ß transforming-growth factor-ß.

DISCUSSION

ER stress has emerged as a key driver of synovitis, not only by amplifying inflammatory signaling [30] but also by promoting fibroblast proliferation [14], angiogenesis [31], and fibrotic remodeling [32] of the synovial tissue. Building on these insights and guided by our previous proteomic approach [18], we investigated in the current study the histological distribution of ER stress proteins in the inflamed human OA synovium. When inflammation was mild (Tak <4), these proteins were primarily localized in the lining layer whereas when the inflammation was severe (Tak ≥4), these proteins were mainly observed in the sublining layer.

Using IMC, we confirmed this pattern of protein infiltration, as well as the corresponding spatial dynamics of fibroblast subsets, although performed on an exploratory cohort with a limited number of samples ($n = 3$). Specifically, under NIN conditions, $CD55^+$ fibroblasts were mainly restricted to the lining layer. In contrast, inflammation was associated with an increased presence of $CD34^+CD31^-$ FLS in the sublining layer. Besides, the distribution of $CD68^+$ (MLS) cells was similar to that of $CD55^+$ cells, but they remained detectable in RA, unlike these cells. These results are consistent with Culemann et al. [3] identifying the presence of a palisade-like shape formed by MLS covering the lining of FLS and generating an internal immunological barrier at the synovial lining. This barrier restricts the inflammatory reaction by providing a tight-junction-mediated barrier that is typically played by epithelial cells in other tissues. Inflammation disrupts cell-to-cell contacts between MLS, thereby altering the structure of the lining layer [3]. RNA-seq data further suggest that FLS undergo a phenotypic switch during synovial inflammation [33]. Lining fibroblasts lose the expression of genes involved in maintaining cellular homeostasis and acquire a pro-inflammatory signature, similar to that of sublining fibroblasts, notably through the secretion of IL-6 [4, 33–35]. We next sought to determine whether the observed patterns of FLS distribution and infiltration were reflected by the expression of the ER stress protein within these cell subsets (CD55, CD34, CD68) across inflammatory grades. The results were consistent with those obtained from a larger cohort using IF. As inflammation progressed, the co-expression of $CD55^+$ FLS in the lining with PDIA4 (the reference ER stress protein) was lost. At the same time, $CD34^+CD31^-$ cells progressively acquired PDIA4 expression as this protein infiltrated the sublining. In other words, as inflammation progressed, the $PDIA4^-$ cells in the sublining decreased progressively, giving way to an expanding $CD34^+CD31^-PDIA4^+$ FLS population. The negative correlation between PDIA4-expressing $CD55^+$ FLS in the lining and PDIA4-expressing $CD34^+$ FLS in the sublining across increasing inflammatory grades, together with the presence of a $CD55^+CD34^+CD31^-$ intermediate FLS subpopulation, points to a continuum of cellular states. This suggests that a gradual phenotypic transition driven by PDIA4 expression is more likely than a binary on/off switch in $PDIA4^+$ cells. Interestingly, no correlation was observed between the two cellular subgroups when they did not express the protein. Consistently, the pro-migratory role of PDIA4 further supports a dynamic, non-binary process underlying fibroblast phenotypic changes. However, these experiments were performed in bulk OA FLS without isolation of $CD55^+$ cells, precluding conclusions on whether this reflects a transition from $CD55^+$ to $CD34^+$ fibroblast subsets. An alternative approach would be to isolate $CD55^+$ FLS and monitor whether their phenotype progressively shifts toward $CD34^+CD31^-$ cells. The key role of FLS in the expression of ER stress proteins aligns with previous data reporting the expression of MANF in FLS. However, this study did not distinguish between the different fibroblast subpopulations [36]. Finally, in our study, ER stress proteins were not expressed in lymphocytes.

We have also demonstrated that HYOU1 and PDIA4 are regulated by UPR pathways in OA FLS. Importantly, the link between UPR signaling and fibrotic processes has been well described in tumor and epithelial cells [37–39], and more recently in OA FLS [32]. Accordingly, we have shown that inhibition of IRE1α and PERK reduces α-SMA expression, supporting a role in fibroblast-to-myofibroblast (FMT) transition. Taken together, these observations suggest that ER stress proteins may contribute to a phenotypic shift of OA FLS toward a proliferative, migratory and pro-fibrotic state, which we therefore sought to investigate under ER stress, pro-inflammatory or pro-fibrotic conditions.

The expression of CD55 or CD34 in FLS was first confirmed in vitro. However, their expression levels remained stable upon stimulation, suggesting that isolated stimuli are insufficient to induce a full phenotypic switch. The expression of studied chaperone proteins (except for BiP) was also observed in FLS without stimulation contributing to cell homeostasis. In contrast, their overexpression was highlighted under these conditions, leading to their secretion for some of them during prolonged ER stress. Interestingly, several chaperones are known to exhibit pro-inflammatory properties when they are exposed to the cell membrane or secreted outside, thereby favoring the production of inflammatory cytokines [12, 13]. This suggests their involvement in triggering arthritis, particularly when they are released. Among these proteins, BiP [40], HSP90B1 [13], PDIA4 [41], ERP29 [42] and CALR [12] have already been described as secreted. In vitro, we demonstrated that human FLS overexpressed BiP, HYOU1, and MANF under ER stress, pro-inflammatory, and pro-fibrotic conditions (Supplementary Table 3). Additionally, PDIA4 and CALR were overexpressed and secreted in vitro by human FLS under prolonged ER stress. PDIA4 was also enhanced under pro-inflammatory conditions, whereas DNAJB11 was overexpressed under the pro-fibrotic process. Based on these findings, we selected the ER stress proteins HYOU1, MANF, PDIA4, DNAJB11 and CALR for further investigation into their role in driving proliferative processes in FLS. HYOU1 promotes the survival of neurons and phagocytes. It is also overexpressed in fibrotic kidneys, while it can be protective in certain fibrotic conditions [43–47]. HYOU1 is also linked to FMT and cytokine production in synovial fibroblasts [48] and has been reported to be over-expressed in injured synovium [49], supporting a role in synovial activation. MANF promotes neuronal survival, suppresses NF-κB–mediated inflammation—particularly in fibroblasts—and reduces fibrosis in the liver [50–55]. It is increased in autoimmune diseases and involved in FLS from proliferative synovium [36, 56]. PDIA4 and DNAJB11 are both linked to inflammation and fibrosis in various tissues, including the lungs, gut, adipose tissue, and

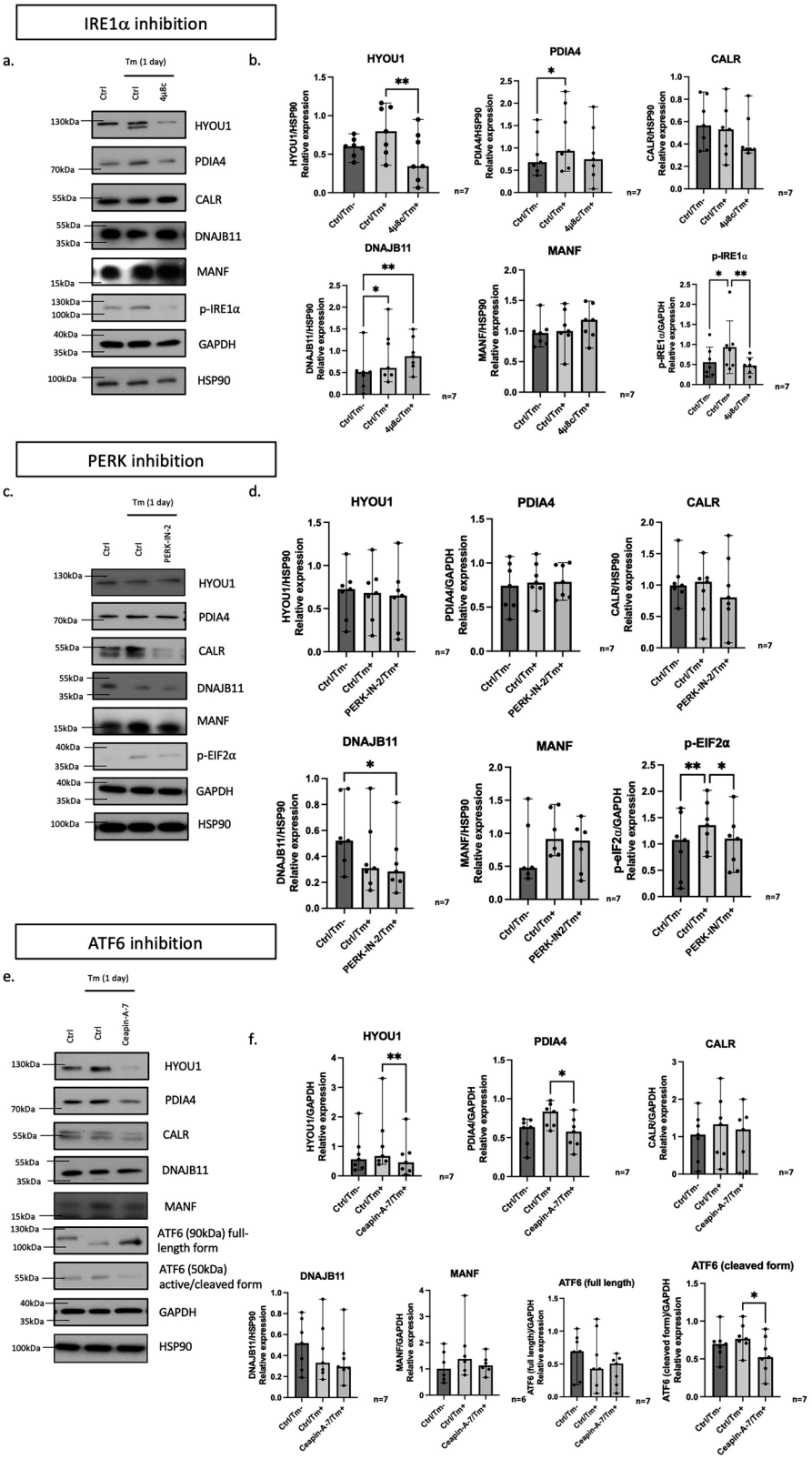

Fig. 7 UPR-dependent regulation of ER stress proteins in OA FLS. To investigate the regulatory pathways involved in the modulation of the five ER stress proteins, cells were pretreated with selective inhibitors of IRE1α (4 μ8c), PERK (PERK-IN-2) or ATF6 (Ceapin-A7) prior to a 1-day tunicamycin stimulation. Pathway inhibition was assessed by monitoring p-IRE1α, EIF2α phosphorylation or cleaved ATF6 (~ 50 kDa). **a**, **c**, **e** Representative Western blots and **b**, **d**, **f**) their corresponding quantifications for IRE1α (4 μ8c), PERK (PERK-IN-2), and ATF6 (Ceapin-A7) inhibition, respectively. Statistical analysis was performed with the nonparametric paired Friedman test followed by Dunn's post hoc test for multiple comparisons. Statistical differences were considered for p values < 0.05 (*$p < 0.05$, **$p < 0.01$, ***$p < 0.001$). Data are presented as median with 95% CI; each point represents one patient. n indicates the number of independent patients. UPR unfolded protein response, OA osteoarthritis, FLS fibroblast-like synoviocytes.

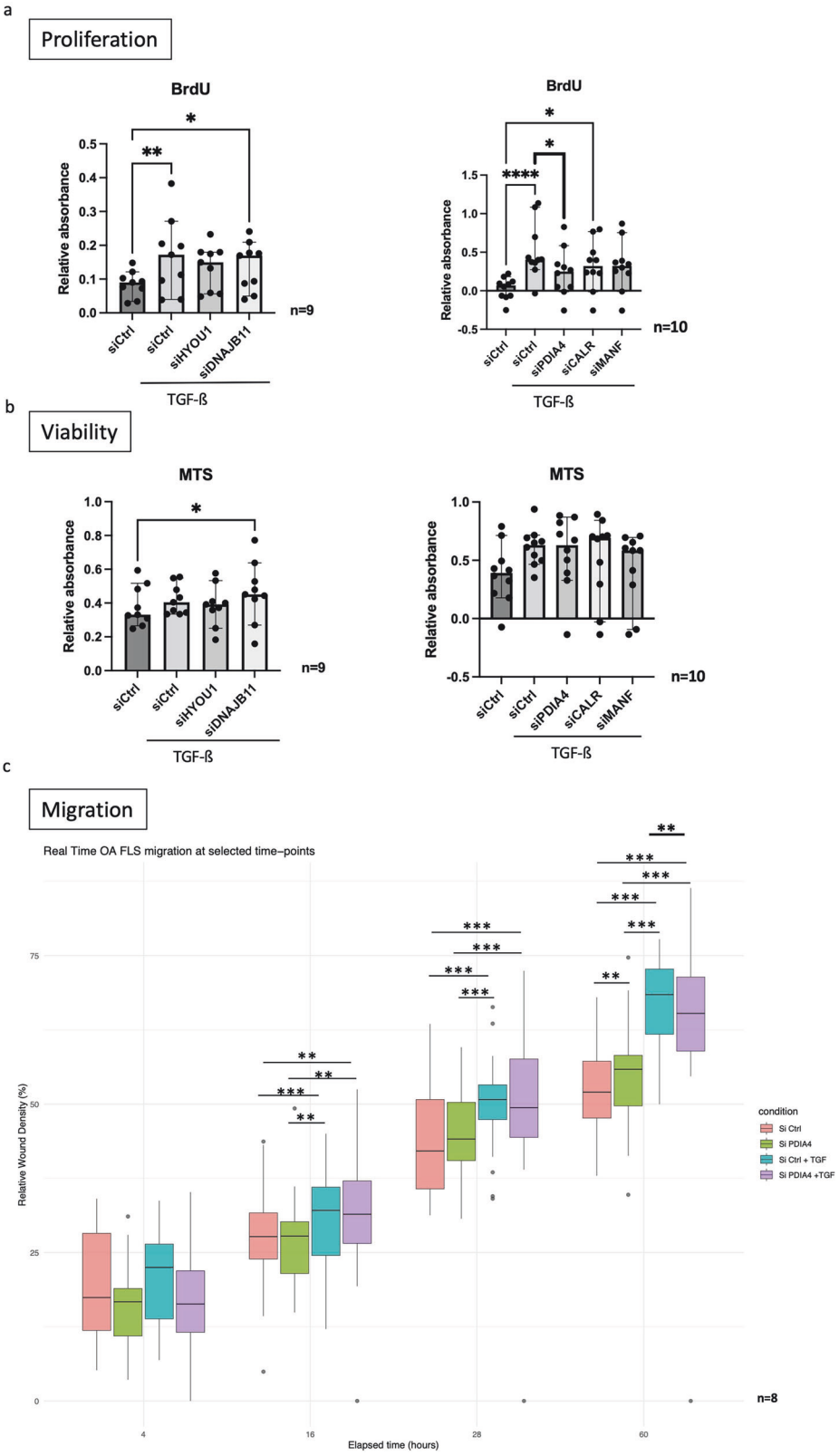

skeletal muscle [57–61]. In particular, PDIA4 negatively regulates the onset of arthritis [62], while DNAJB11 has been associated with autosomal-dominant polycystic kidney disease involving fibrosis [63, 64], but remains unexplored in synovial pathology. Finally, CALR, which is overexpressed in RA synovium, contributes to FLS survival and angiogenesis [65–68] and has been identified as a stromal-derived antigen in RA synovial cells [66], highlighting it as a potential key target in synovitis.

HYOU1, MANF, PDIA4, DNAJB11, and CALR have previously been identified as having pro-proliferative effects in tumor cells,

Fig. 8 Effect of ER stress protein silencing on FLS proliferation, viability and migration. a FLS were transfected with siRNAs targeting HYOU1, MANF, PDIA4, DNAJB11, or CALR, then stimulated with TGF-β (10 ng/mL) for 3 days. Proliferation was measured by BrdU incorporation, and **b** viability by MTS assay. Data are presented as median with 95% CI; each point represents one patient. Statistical significance was assessed using the nonparametric paired Friedman test followed by Dunn's post hoc test for multiple comparisons. n indicates the number of independent patients. **c** Real-time migration of OA FLS monitored using the IncuCyte system. Cells were transfected with control siRNA (siCtrl) or siRNA targeting PDIA4 (siPDIA4), with or without a 3-day TGF-β stimulation. Migration was quantified as relative wound density (%) at the indicated time points (hours). Migration data were analyzed using linear mixed-effects models with treatment, time, and their interaction as fixed effects and patient as a random effect. Statistical differences were considered for p values < 0.05: *$p < 0.05$, **$p < 0.01$, ***$p < 0.001$ and ****$p < 0.0001$); FLS fibroblast-like synoviocytes, Ctrl controls. ER endoplasmic reticulum, TGF-ß transforming-growth factor-ß, siRNA small interfering, BrdU bromodésoxyuridine.

promoting cell survival and invasive behavior [69–73]. Synovitis is characterized by hyperplasia (cell proliferation) and inflammation that can lead to fibrosis in a chronic condition. This characteristic was investigated in FLS previously stimulated with TGF-β, in which the five ER stress proteins were silenced. Among them, PDIA4 was found to promote FLS proliferation in OA. This is the first study to describe the role of PDIA4 in the proliferation of OA FLS.

In conclusion, chaperones are detected in the lining layer of the synovial membrane under mild inflammatory conditions. As inflammation increases and the lining becomes disrupted, these ER stress proteins are expressed at higher levels by cells in the sublining. These proteins are expressed by $CD55^+$ FLS and $CD68^+$ MLS (NIN OA) in the lining, and by $CD34^+CD31^-$ FLS in the sublining (IN OA), and may be linked to the transition of their phenotype towards the deeper synovial layers. In vitro experiments using FLS further demonstrated that PDIA4 may be actively involved in proliferative and migratory processes, contributing to synovitis and OA disease progression, although its in vivo role in synovitis progression remains to be established.

This study provides the first spatial and functional characterization of ER stress proteins in synovitis. It links ER stress to fibroblast plasticity and reveals an association between chaperones and proliferative, migratory and pro-fibrotic processes in OA synovitis. Although restricted to OA-derived FLS, similar ER stress–driven mechanisms may also occur in RA and other inflammatory arthropathies.

DATA AVAILABILITY

The datasets generated during and/or analyzed during the current study are available from the corresponding author on reasonable request.

REFERENCES

1. Smith MD. The normal synovium. Open Rheumatol J. 2011;5:100–6.
2. Mathiessen A, Conaghan PG. Synovitis in osteoarthritis: current understanding with therapeutic implications. Arthritis Res Ther. 2017;19:18.
3. Culemann S, Grüneboom A, Nicolás-Ávila JA, Weidner D, Lämmle KF, Rothe T, et al. Locally renewing resident synovial macrophages provide a protective barrier for the joint. Nature. 2019;572:670–5.
4. Labinsky H, Panipinto PM, Ly KA, Khuat DK, Madarampalli B, Mahajan V, et al. Multiparameter analysis identifies heterogeneity in knee osteoarthritis synovial responses. Arthritis Rheumatol. 2020;72:598–608.
5. Zhang F, Wei K, Slowikowski K, Fonseka CY, Rao DA, Kelly S, et al. Defining inflammatory cell states in rheumatoid arthritis joint synovial tissues by integrating single-cell transcriptomics and mass cytometry. Nat Immunol. 2019;20:928–42.
6. Smith MH, Gao VR, Periyakoil PK, Kochen A, DiCarlo EF, Goodman SM, et al. Drivers of heterogeneity in synovial fibroblasts in rheumatoid arthritis. Nat Immunol. 2023;24:1200–10.
7. Croft AP, Campos J, Jansen K, Turner JD, Marshall J, Attar M, et al. Distinct fibroblast subsets drive inflammation and damage in arthritis. Nature. 2019;570:246–51.
8. Stephenson W, Donlin LT, Butler A, Rozo C, Bracken B, Rashidfarrokhi A, et al. Single-cell RNA-seq of rheumatoid arthritis synovial tissue using low-cost microfluidic instrumentation. Nat Commun. 2018;9:791.
9. Kohno K. How transmembrane proteins sense endoplasmic reticulum stress. Antioxid Redox Signal. 2007;9:2295–303.
10. Daverkausen-Fischer L, Draga M, Pröls F. Regulation of translation, translocation, and degradation of proteins at the membrane of the endoplasmic reticulum. Int J Mol Sci. 2022;23:5576.
11. Zhang K, Kaufman RJ. From endoplasmic-reticulum stress to the inflammatory response. Nature. 2008;454:455–62.
12. Duo CC, Gong FY, He XY, Li YM, Wang J, Zhang JP, et al. Soluble calreticulin induces tumor necrosis factor-α and interleukin-6 production by macrophages through MAPK and NF-κB signaling pathways. Int J Mol Sci. 2014;15:2916–28.
13. Huang QQ, Sobkoviak R, Jockheck-Clark AR, Shi B, Mandelin AM, Tak PP, et al. Heat shock protein 96 is elevated in rheumatoid arthritis and activates macrophages primarily via TLR2 signaling. J Immunol. 2009;182:4965–73.
14. Yoo SA, You S, Yoon HJ, Kim DH, Kim HS, Lee K, et al. A novel pathogenic role of the ER chaperone GRP78/BiP in rheumatoid arthritis. J Exp Med. 2012;209:871–86.
15. Connor AM, Mahomed N, Gandhi R, Keystone EC, Berger SA. TNFα modulates protein degradation pathways in rheumatoid arthritis synovial fibroblasts. Arthritis Res Ther. 2012;14:R62.
16. Wang L, Fan Y, Gui Y, Yang X, Ye X, Cao Y, et al. Endoplasmic reticulum stress triggered autophagy and regulated phenotype transformation of rheumatoid arthritis synovial fibroblasts via the IRE1/JNK pathway. Ann Transl Med. 2022;10:725.
17. Rahmati M, Moosavi MA, McDermott MF. ER stress: a therapeutic target in rheumatoid arthritis?. Trends Pharm Sci. 2018;39:610–23.
18. de Seny D, Bianchi E, Baiwir D, Cobraiville G, Collin C, Deliège M, et al. Proteins involved in endoplasmic reticulum stress are modulated in synovitis and correlate with the histological inflammatory score. Sci Rep. 2020;10:70803.
19. Tak PP, Thurkow EW, Daha MR, Kluin PM, Smeets TJ, Meinders AE, et al. Expression of adhesion molecules in early rheumatoid synovial tissue. Clin Immunol Immunopathol. 1995;77:236–42.
20. Deroyer C, Poulet C, Paulissen G, Ciregia F, Malaise O, Plener Z, et al. CEMIP regulates inflammation, hyperplasia and fibrosis in osteoarthritis synovial membrane. Cell Mol Life Sci. 2022;79:282.
21. Ma HL, Blanchet TJ, Peluso D, Hopkins B, Morris EA, Glasson SS. Osteoarthritis severity is sex dependent in a surgical mouse model. Osteoarthr Cartil. 2007;15:695–700.
22. Thysen S, Luyten FP, Lories RJU. Targets, models and challenges in osteoarthritis research. Dis Model Mech. 2015;8:17–30.
23. Bankhead P, Loughrey MB, Fernández JA, Dombrowski Y, McArt DG, Dunne PD, et al. QuPath: open source software for digital pathology image analysis. Sci Rep. 2017;7:16878.
24. Deroyer C, Charlier E, Neuville S, Malaise O, Gillet P, Kurth W, et al. CEMIP induces a fibrosis-like process in osteoarthritic chondrocytes. Cell Death Dis. 2019;10:103.
25. Paulissen G, Malaise O, Deroyer C, Charlier E, Neuville S, Plener Z, et al. JAK inhibitors alleviate metabolic dysregulation, inflammation and fibrosis in osteoarthritis. Rheumatol (Oxf). 2025;64:5539–50.
26. Feng LJ, Jiang TC, Zhou CY, Yu CL, Shen YJ, Li J, et al. Activated macrophage-like synoviocytes are resistant to endoplasmic reticulum stress-induced apoptosis. Inflamm Res. 2014;63:335–46.
27. Sohn C, Lee A, Qiao Y, Loupasakis K, Ivashkiv LB, Kalliolias GD. Prolonged tumor necrosis factor α primes fibroblast-like synoviocytes by altering chromatin. Arthritis Rheumatol. 2015;67:86–95.
28. Baba T, Ishizu A, Iwasaki S, Suzuki A, Tomaru U, Ikeda H, et al. CD4+/CD8+ macrophages infiltrating inflammatory sites: a cytotoxic phenotype. Blood. 2006;107:2004–12.
29. Raposo RAS, Thomas B, Ridlova G, James W. Proteomic-based identification of CD4-interacting proteins in macrophages. PLoS One. 2011;6:e18690.
30. Qiu Q, Zheng Z, Chang L, Zhao YS, Tan C, Dandekar A, et al. Toll-like receptor-mediated IRE1α activation as a therapeutic target for inflammatory arthritis. EMBO J. 2013;32:2477–90.
31. Katanasaka Y, Ishii T, Asai T, Naitou H, Maeda N, Koizumi F, et al. Cancer anti-neovascular therapy targeting BiP/GRP78. Int J Cancer. 2010;127:2685–98.
32. Ding L, Liao T, Yang N, Wei Y, Xing R, Wu P, et al. Chrysin ameliorates synovitis and fibrosis via PERK signaling. Front Pharm. 2023;14:1170243.

33. Armaka M, Konstantopoulos D, Tzaferis C, Lavigne MD, Sakkou M, Liakos A, et al. Single-cell multimodal analysis identifies regulatory programs. Genome Med. 2022;14:78.
34. Smith MH, Gao VR, Periyakoil PK, Kochen A, DiCarlo EF, Goodman SM, et al. Drivers of heterogeneity in synovial fibroblasts. Nat Immunol. 2023;24:1200–10.
35. Miyahara J, Omata Y, Chijimatsu R, Okada H, Ishikura H, Higuchi J, et al. CD34hi subset contributes to fibrotic phenotype. JCI Insight. 2025;10:e183690.
36. Chen L, Feng L, Wang X, Du J, Chen Y, Yang W, et al. Mesencephalic astrocyte-derived neurotrophic factor is involved in inflammation by negatively regulating the NF-κB pathway. Sci Rep. 2015;5:8133.
37. Tanjore H, Cheng DS, Degryse AL, Zoz DF, Abdolrasulnia R, Lawson WE, et al. Alveolar epithelial cells undergo epithelial-to-mesenchymal transition in response to endoplasmic reticulum stress. J Biol Chem. 2011;286:30972–80.
38. Matsuzaki S, Hiratsuka T, Taniguchi M, Shingaki K, Kubo T, Kiya K, et al. Physiological ER stress mediates the differentiation of fibroblasts. PLoS One. 2015;10:e0123578.
39. Shin HS, Ryu ES, Oh ES, Kang DH. Endoplasmic reticulum stress as a target to ameliorate epithelial-to-mesenchymal transition and apoptosis. Lab Invest. 2015;95:1157–73.
40. Peters LR, Raghavan M. Endoplasmic reticulum calcium depletion impacts chaperone secretion, innate immunity, and phagocytosis. J Immunol. 2011;187:919–31.
41. Turano C, Coppari S, Altieri F, Ferraro A. Proteins of the PDI family: unpredicted non-ER locations and functions. J Cell Physiol. 2002;193:154–63.
42. Holbrook LM, Watkins NA, Simmonds AD, Jones CI, Ouwehand WH, Gibbins JM. Platelets release thiol isomerase enzymes following activation. Br J Haematol. 2010;148:627–37.
43. Tamatani M, Matsuyama T, Yamaguchi A, Mitsuda N, Tsukamoto Y, Taniguchi M, et al. ORP150 protects against hypoxia/ischemia-induced neuronal death. Nat Med. 2001;7:317–23.
44. Nakagomi T, Kitada O, Kuribayashi K, Yoshikawa H, Ozawa K, Ogawa S, et al. The 150-kDa oxygen-regulated protein ameliorates acute lung injury. Am J Pathol. 2004;165:155–64.
45. Lindenmeyer MT, Rastaldi MP, Ikehata M, Neusser MA, Kretzler M, Cohen CD, et al. Proteinuria and hyperglycemia induce endoplasmic reticulum stress. J Am Soc Nephrol. 2008;19:2225–36.
46. Kademani SP, Nelaturi P, Kalidas SS, Ballambattu VB, Sambandam R. Urinary biomarkers of chronic kidney disease. Indian J Nephrol. 2025;35:253–8.
47. Dihazi H, Dihazi GH, Mueller C, Lahrichi L, Asif AR, Bibi A, et al. Proteomics characterization of fibrosis phenotype. J Proteom. 2011;74:304–18.
48. Papadopoulou D, Mavrikaki V, Charalampous F, Tzaferis C, Samiotaki M, Papavasileiou KD, et al. Inhibitors of HYOU1 suppress fibroblast activation. Angew. Chem Int Ed Engl. 2024;63:e202319157.
49. Yuan T, Qian H, Yu X, Meng J, Lai CT, Jiang H, et al. Proteomic analysis reveals rotator cuff injury caused by oxidative stress. Ther Adv Chronic Dis. 2021;12:2040622320987057.
50. Eesmaa A, Yu LY, Göös H, Nõges K, Kovaleva V, Hellman M, et al. MANF promotes neuronal survival independently from GRP78. J Biol Chem. 2021;296:100295.
51. Neves J, Zhu J, Sousa-Victor P, Konjikusic M, Riley R, Chew S et al. Immune modulation by MANF promotes tissue repair and regeneration. Science. 2016;353, aaf3646.
52. Gong L, Dong J, Huang K, Pan K, Wang S, Liu H. MANF regulates inflammatory response in fibroblasts. Eur J Oral Sci. 2023;131:e12945.
53. Pi Z, Wu Y, Wang X, Li P, Wang R. Exosomal MANF regulates osteoclast differentiation. J Orthop Surg Res. 2025;20:349.
54. Sousa-Victor P, Neves J, Cedron-Craft W, Ventura PB, Liao CY, Riley RR, et al. MANF regulates metabolic and immune homeostasis. Nat Metab. 2019;1:276–90.
55. Tao X, Wang D, Liang Y, Yang L, He E, Zhou J, et al. PRDX6 inhibits fibrosis via MANF secretion. Biomed Pharmacother. 2022;156:113931.
56. Cheng D, Zhou T, Liu H, Li L, Xuan Y, Huang L, et al. MANF inhibits apoptosis in Sjögren's syndrome. Int Immunopharmacol. 2023;122:110582.
57. Li H, Liu Q, Xiao K, He Z, Wu C, Sun J, et al. PDIA4 correlates with poor prognosis in glioma. Onco Targets Ther. 2021;14:125–38.
58. Weidner J, Jarenbäck L, Åberg I, Westergren-Thorsson G, Ankerst J, Bjermer L, et al. ER and Golgi disorganization in fibroblasts. Physiol Rep. 2018;6:e13584.
59. Negroni A, Prete E, Vitali R, Cesi V, Aloi M, Civitelli F, et al. ER stress in inflammatory bowel disease. Dig Liver Dis. 2014;46:788–94.
60. Su SC, Chien CY, Chen YC, Chiang CF, Lin FH, Kuo FC, et al. PDIA4 modulates adiponectin expression and inflammation. Biofactors. 2022;48:1060–75.
61. Lee AS. Glucose-regulated proteins in cancer: molecular mechanisms and therapeutic potential. Nat Rev Cancer. 2014;14:263–76.
62. Yang A, Lin L, Zhang J, Wu Y, Zhao Z. ERp72 in autoantibody-induced arthritis. Scand J Rheumatol. 2025;54:16–24.
63. Cornec-Le Gall E, Olson RJ, Besse W, Heyer CM, Gainullin VG, Smith JM, et al. DNAJB11 mutations cause atypical polycystic kidney disease. Am J Hum Genet. 2018;102:832–44.
64. Elhassan EAE, O'Donoghue D, Heneghan S, Teltsh O, Sarihan S, Osman SM et al. Phenotypic outcomes in autosomal dominant polycystic kidney disease. J Nephrol. 2025 https://doi.org/10.1007/s40620-024-02184-3.
65. Ding H, Hong C, Wang Y, Liu J, Zhang N, Shen C, et al. Calreticulin promotes angiogenesis via nitric oxide signaling. Clin Exp Immunol. 2014;178:236–44.
66. Corsiero E, Caliste M, Jagemann L, Fossati-Jimack L, Goldmann K, Cubuk C, et al. Autoimmunity to stromal-derived autoantigens exacerbates arthritis. J Clin Invest. 2024;134:e169754.
67. Jiao Y, Ding H, Huang S, Liu Y, Sun X, Wei W, et al. Calreticulin promotes apoptosis resistance in rheumatoid arthritis synoviocytes. Clin Exp Rheumatol. 2018;36:123–31.
68. Hayashi J, Kihara M, Kato H, Nishimura T. Proteomic profile of synoviocyte lesions. Clin Proteom. 2015;12:10.
69. Lindahl M, Danilova T, Palm E, Lindholm P, Võikar V, Hakonen E, et al. MANF is indispensable for pancreatic β-cell survival. Cell Rep. 2014;7:366–75.
70. Xing F, Song Z, Cheng Z. PDIA4 promotes malignant cell behavior in cervical cancer. Oncol Rep. 2022;48:123.
71. Liu P, Zu F, Chen H, Yin X, Tan X. Exosomal DNAJB11 promotes pancreatic cancer development. Cell Mol Biol Lett. 2022;27:87.
72. Miao Y, Wang X, He F, Zhang F, Huang Y, Lai Y, et al. Targeting CALR reduces energy metabolism in cancer cells. Int J Oncol. 2025;66:123.
73. Wang W, Jiang X, Xia F, Chen X, Li G, Liu L, et al. HYOU1 promotes proliferation via PI3K/AKT pathway. Mol Biol Rep. 2023;50:453–64.

ACKNOWLEDGEMENTS

The authors thank the Immunohistochemistry and Imagery platforms of GIGA at the University of Liège for their contribution. The authors acknowledge the cytometry flow core facility Hyperion (Brest, France) for its technical assistance, as well as the European FEDER grant program Progos RU 000950 members of the Scientific Interest Group (GIS) Biogenouest.

AUTHOR CONTRIBUTIONS

ZG and D de Seny conceived and designed the experiments. ZG, SN, ZP, PS, PH, YD, NM, and GC performed the experiments. ZG, CP, AH, GL, GC, and Dde Seny analysed the data. CDaniel, TT, TS, PDurez, EB, and PDelvenne provided joint tissues and FFPE synovial membranes and characterized synovial membrane inflammation. ZG and D de Seny wrote the manuscript. ZG, PS, AH, CDeroyer, CP, GP, GC, CR, and Dde Seny contributed to the conception of the study and to drafting the manuscript. All authors read and approved the final manuscript.

FUNDING

This study was supported by the "Fond d'Investissement pour la Recherche Scientifique" (FIRS, Center Hospitalier Universitaire de Liège, Belgium), the Fondation Lejeune-Lechien, the Fondation Arthrose, and a clinical research grant (Léon Frédéricq, Belgium) and the "Organisation Belge CAP48". ZG is funded by the "Fonds National de la Recherche Scientifique" (FNRS).

COMPETING INTERESTS

The authors declare no competing interests.

ETHICAL APPROVAL AND INFORMED CONSENT

All experiments were undertaken with patient material complying with the regulations and ethical guidelines of the University Hospital of Liège (CHU) and Catholic University of Louvain (UCLouvain) Belgium, and were approved by the CHU ethical committee (ref: 2017/147) and UCLouvain ethical committee (ref: 2013/24MAI/293) and the biobank research committee (BB190058) of the CHU of Liège. We certify that the study was conducted under the ethical standards outlined in the 1964 Declaration of Helsinki and its subsequent amendments, or with comparable ethical standards. Informed consent was obtained from all individual participants included in the study. All animal studies were conducted in compliance with European and Belgian guidelines for the care and use of laboratory animals, and experimentation procedures were approved by the local ethical committee (LA1610002; #14-1721 University of Liège, Liège, Belgium). The experiments comply with the current laws of

Belgium in which they were performed. Investigators were not blinded to group allocation.

ADDITIONAL INFORMATION

Supplementary information The online version contains supplementary material available at https://doi.org/10.1038/s41418-026-01841-3.

Correspondence and requests for materials should be addressed to Dominique de Seny.

Reprints and permission information is available at http://www.nature.com/reprints

Publisher's note Springer Nature remains neutral with regard to jurisdictional claims in published maps and institutional affiliations.